Supporting Information

Molecular in situ monitoring of pH-triggered response in adaptive polymers by two-dimensional Raman micro-correlation-spectroscopy

*Julian Hniopek[a,b,c], Josefine Meurer[d,e], Stefan Zechel[d,e], Michael Schmitt[b,c], Martin D. Hager[*d,e], Jürgen Popp[*a,b,c,e]*

---

a. J. Hniopek, Prof. J. Popp
Department Spectroscopy & Imaging, Leibniz Institute of Photonic Technology, Albert-Einstein-Str. 9, 0775 Jena, Germany. E-mail: juergen.popp@leibniz-ipht.de

b. J. Hniopek, apl. Prof. M. Schmitt, Prof. J. Popp
Institute of Physical Chemistry (IPC), Friedrich Schiller University Jena, Helmholtzweg 4, 07743 Jena, Germany

c. J. Hniopek, apl. Prof. M. Schmitt, Prof. J. Popp
Abbe Center of Photonics, Friedrich Schiller University Jena, Albert-Einstein-Str. 6, 07745 Jena, Germany

d. J. Meurer, Dr. S. Zechel, Dr. M. D. Hager
Laboratory of Organic and Macromolecular Chemistry (IOMC), Friedrich Schiller University Jena, Humboldtstr. 10, 07743 Jena, Germany

e. J. Meurer, Dr. S. Zechel, Dr. M. D. Hager, Prof. Dr. J. Popp
Jena Center of Soft Matter (JCSM), Friedrich Schiller University Jena, Philosophenweg 7, 07743 Jena, Germany

Table of Contents

Synthetic Procedures

Synthesis of 4-Formylphenyl-methacrylate (1)

The synthesis of 4-formylphenyl-methacrylate (1) was adapted from literature procedures.[1, 2] For the detailed reaction scheme see Scheme S1a.

The reaction was performed under nitrogen atmosphere. First, 4-hydroxybenzaldehyde (10.0 g, 81.89 mmol) was added into a two-neck-round-bottom-flask and was dissolved in dichloromethane (100 mL). Subsequently, triethyl amine (14.9 mL, 106.45 mmol) was added. The resulting mixture was cooled to 0 °C and a solution of methacryloyl chloride (8.7 mL, 90.08 mmol) in dichloromethane (20 mL) was added dropwise under stirring. After the addition, the reaction mixture was stirred at room temperature overnight. Subsequently, the solution was washed three times with a saturated aqueous solution of $NaHCO_3$ and two times with water. The dichloromethane phase was dried over Na_2SO_4 and the solvent was removed *in vacuo*. The resulting crude product was purified *via* gel chromatography (silica/chloroform, rf = 0.5).

Yield: 14.83 g of colorless oil, 95% (Lit.: 91%)[1, 2]

^{1}H NMR (300 MHz, CD_2Cl_2) δ = 9.99 (s, 1H, -CHO), 7.98 – 7.86 (m, 2H, Ar-H), 7.32 (d, *J* = 8.5 Hz, 2H, Ar-H), 6.39 – 6.34 (m, 1H, =CH_2), 5.89 – 5.72 (m, 1H, =CH_2), 2.06 (dd, *J* = 1.5, 1.0 Hz, 3H, CH_3) ppm.

Synthesis of the Polymers P1 and P2

Both polymerizations were performed *via* a free radical polymerization (FRP) with 2,2'-azobis(2-methylpropionitrile) (AIBN) as initiator. The reaction scheme is presented in **Scheme S1b**. The monomer to initiator ratio was 100 to 1. Into a 20 mL microwave vial (**P1**), respectively a 100 mL one-neck-round-bottom-flask (**P2**), the former synthesized monomer **1** and AIBN were added. For the synthesis of the copolymer **P2** additionally MMA (3.16 g) was added. Afterwards, *N,N*-dimethyl formamide was added until a monomer concentration of 2 mol L^{-1} was reached. The reaction mixtures were purged for 30 minutes with nitrogen before they were stirred overnight at a temperature of 70 °C in a preheated oil bath. Afterwards, the solvent was removed *in vacuo*. The residuals were dissolved in a small amount of chloroform (5 to 10 mL) and precipitated in cold diethyl ether. The obtained polymers were filtered, washed twice with cold diethyl ether and dried *in vacuo* at a temperature of about 40 °C. Both polymers were characterized by ^{1}H NMR spectroscopy and size exclusion chromatography (SEC).

The utilized quantities of all substances are listed in Table S1.

Table S1: Utilized quantities and voluminal of all substances for the synthesis of **P1** and **P2** *via* FRP.

	1		**MMA**		**AIBN**		**DMF**
	n [mmol]	m [g]	n [mmol]	m [g]	n [mmol]	m [mg]	V [mL]
P1	15.773	3.0	-	-	0.158	25.9	7.9
P2	31.546	6.0	31.546	3.16	0.631	103.6	31.5

P1:

Yield: 1.43 g
^{1}H NMR (300 MHz, CD_2Cl_2) δ = 9.92 (1H, -C*H*O), 7.82 (2H, Ar-*H*), 7.25 (2H, Ar-*H*), 2.29 – 0.88 (5H, polymer backbone).
SEC DMAc/LiCl, PMMA standard): M_n = 26,900 g mol^{-1}, M_w = 160,200 g mol^{-1}, Đ = 5.95.

P2:

Yield: 6.30 g
^{1}H NMR (300 MHz, CD_2Cl_2) δ = 9.97 (1H, -C*H*O), 7.89 (2H, Ar-*H*), 7.29 (2H, Ar-*H*), 3.56 (3H, OCH_2), 2.12 – 0.83 (11H, polymer backbone).
SEC ($CHCl_3$/NEt_3DMAc/LiCl, PMMA standard): M_n = 35,600 g mol^{-1}, M_w = 134,700 g mol^{-1}, Đ = 3.78.

Synthesis of the Functionalized Polymers P3 and P4
The protocol for the functionalization of both polymers was adapted from literature procedure.[1, 2] **Scheme S1c** is summarizing the functionalization of both polymers with the amine. The utilized quantities of all substances are listed in **Table S2**.

First, polymer **P1** and polymer **P2**, respectively, were added into a 100 mL one-neck-round-bottom-flask and were dissolved in dichloromethane. Subsequently, sodium sulfate was added as desiccant. The mixture was purged with nitrogen for 30 minutes. Subsequently, *n*-butylamine was added and the reaction mixture was stirred at room temperature overnight. Afterwards, the sodium sulfate was removed by filtration. The pure polymers were obtained *via* preparative SEC (BioBeads® SX1 swollen in chloroform) and characterized by ^{1}H NMR spectroscopy and SEC.

Table S2: Utilized quantities of all substances for the synthesis of **P3** and **P4**.

	Polymer		**Butylamine**		**Sodium sulfate**		**CH_2Cl_2**
	Utilized	m [g]	n [mmol]	V [mL]	n [mmol]	m [mg]	V [mL]
P3	**P1**	1.3	8.20	0.81	17.09	2.43	40
P4	**P2**	3.0	20.67	2.04	41.33	5.89	50

P3:

Yield: 0.8 g
^{1}H NMR (300 MHz, CD_2Cl_2) δ = 8.18 (1H, -C*H*N), 7.61 (2H, Ar-*H*), 7.14 (2H, Ar-*H*), 3.56 (2H, =N-CH_2), 2.38 – 0.92 (12H, CH_2-CH_2-CH_3, polymer backbone).
SEC (DMAc/LiCl, PMMA standard): M_n = 76,300 g mol^{-1}, M_w = 635,600 g mol^{-1}, Đ = 7.84.

P4:

Yield: 2.8 g
^{1}H NMR (300 MHz, CD_2Cl_2) δ = 8.23 (1H, -C*H*N), 7.70 (2H, Ar-*H*), 7.13 (2H, Ar-*H*), 3.58 (5H, =N-CH_2, OCH_3), 2.37 – 0.73 (18H, CH_2-CH_2-CH_3, polymer backbone).
SEC (DMAc/LiCl, PMMA standard): M_n = 37,800 g mol^{-1}, M_w = 165,400 g mol^{-1}, Đ = 4.37.

Swelling experiment of P3 and P4

For the determination of the swelling degree, a defined mass of the polymer, **P3** or **P4** ($m_{polymer}$), was filled into a 3 mL vial. Subsequently, 1 mL of a mixture based on water and concentrated acetic acid (V/V = 9/1) was added. After 1 h the swollen polymer was filtered to determine its mass ($m_{swollen}$). All determined values are listed in **Table SX**. The swelling degree (SD) was calculated according to Equation S1.

$$SD = \frac{m_{swollen} - m_{polymer}}{m_{polymer}} \times 100\% \quad \text{(S1)}$$

Table SX: Determined masses for the calculation of the swelling degree for **P3** and **P4**.

Sample	Test 1			Test 2		
	$m_{polymer}$ [mg]	$m_{swollen}$ [mg]	SD [%]	$m_{polymer}$ [mg]	$m_{swollen}$ [mg]	SD [%]
P3	24	385	1500	15	183	1120
P4	29	93	221	26	90	246

Raman spectroscopy

Processing and calculation details

Preprocessing routine

Before further analysis, all Raman spectra were preprocessed using in-house developed scripts written in the programming language R.[3] First, the wavenumber region was restricted to the range of 200 – 3200 cm^{-1} for the Fourier transform Raman spectra at 1064 nm and 500 – 2600 cm^{-1} for the Raman microscopy data recorded at 514 nm excitation wavelength. Next, to suppress the influence of varying baseline due to fluorescence, a SNIP based background correction was performed using 40 iterations with a window of 3 and smoothing enabled on the baseline.[4] Afterwards, the spectra were normalized using Euclidean vector norm. For the images, the spectra laterally separated by 10 µm in each depth were averaged to minimize lateral variations.

Calculation of band areas

For the calculation of the band areas shown in Figure 2 in the main manuscript, the signal intensities in the areas between 1700 – 1720 (vC=O) respectively 2100 – 2120 cm^{-1} (vC-D) were summed up. Since the spectra in each depth were not recorded at the same time during the scan (since each point measurement took 2 seconds, cf. **Figure S1**) interpolation along the time axis was necessary for further analysis and illustration. Therefore, the intensity values at each point were linearly interpolated onto the same 0 – 400 s timescale with 20 s step size for all points using the *approx* function of R. As input values for the interpolated times, the mean time delay of each layer with respect to the first point recorded in a certain set of spectra was used (1 – 15 s, 4s steps, cf. Table S3).

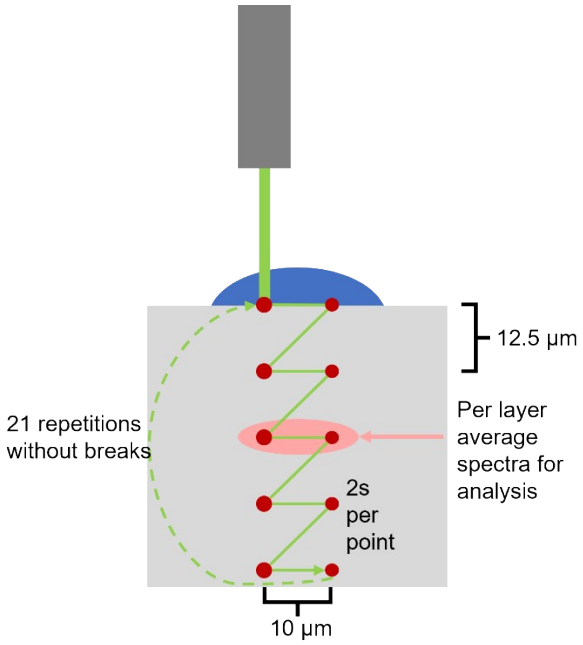

Figure S1: Schematic depiction of the confocal Raman microscopy measurement scheme.

Table S3: Time delays of each depth with respect to the first point of each depth scan (z/x=0 µm)

Depth		**0 µm**	**12.5 µm**	**25 µm**	**37.5 µm**	**50 µm**
Time offset	**x = 0 µm / x = 10 µm**	0 / 2 s	4 / 6 s	8 / 10 s	12 / 14 s	16 / 18 s
	Mean	1 s	5 s	9 s	13 s	15 s

Calculation of hydrolyzation ratios

For the calculation of the hydrolyzation ratios of the polymer, the signal intensities of the imine band (1645 – 1665 cm^{-1}) and a polymer backbone C-C band at centered at 1220 cm^{-1} (area 1210 – 1230 cm^{-1}) were summed up. The backbone C-C band is not affected by the hydrolyzation and, thus, can serve as an internal standard.

The ratio of the imine to backbone C-C band area for unhydrolyzed polymer was determined to be 1.63 using the t=0 measurements for depths > 12.5 µm. The ratio of imine to C-C backbone was then calculated for each measurement point in the experiment, affording the traces depicted in **Figure S2**. As described in the manuscript, the ratio of imine to backbone is not decreasing consistently but starts to increase again after a minimum. This finding can be explained by some swelling discussed in the manuscript. From the minimum imine ratio, the hydrolyzation ratio can be calculated by simply subtracting it from 1, resulting in hydrolyzation ratios of 65% to 81%. The lower maximum amounts for points in smaller depths are probably also caused by the swelling, which has a stronger effect on points with a lower depth, as there is more material under the respective spot that can swell.

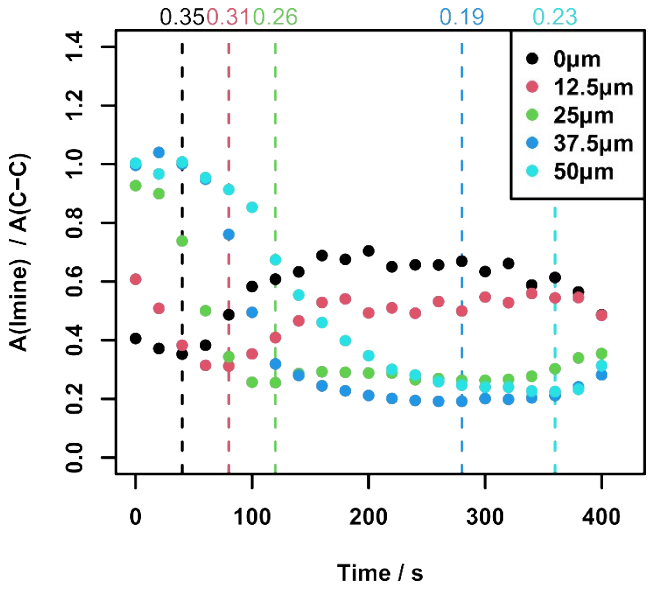

Figure S2: Band area ratios of Imine (1645 – 1665 cm^{-1}) and C-C bands (1210 – 1230 cm^{-1}) in all depths over a time span of 400 s. The ratios are normalized to the band ratio in pristine polymer (A_{Imine} / A_{C-C} = 1.63)

Additional Raman spectra

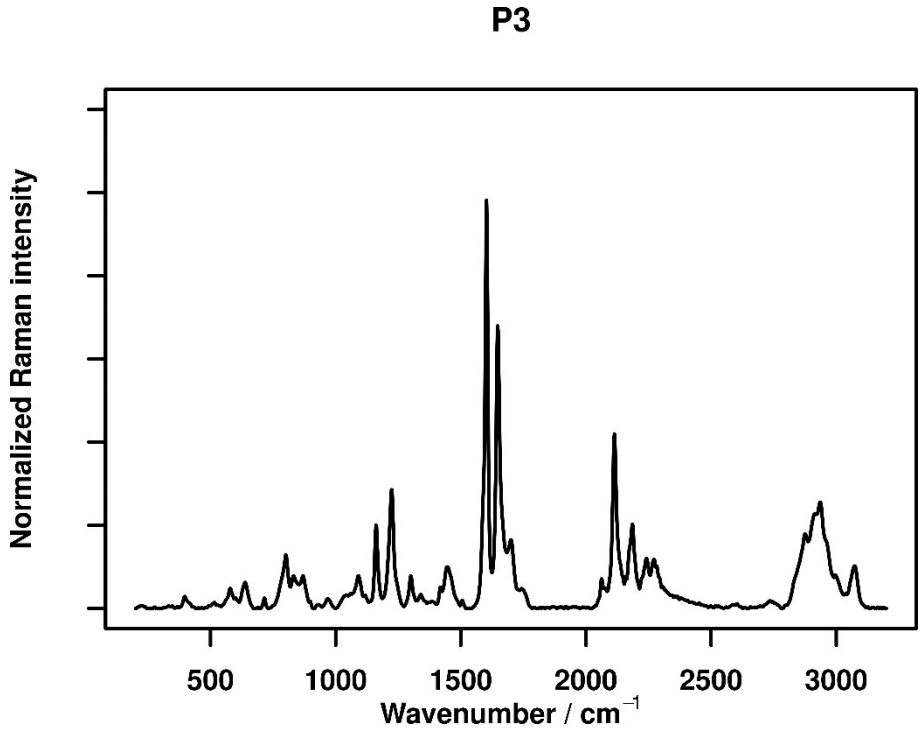

Figure S3: FT-Raman spectrum of P3 in the range of 200 – 3200 cm^{-1}.

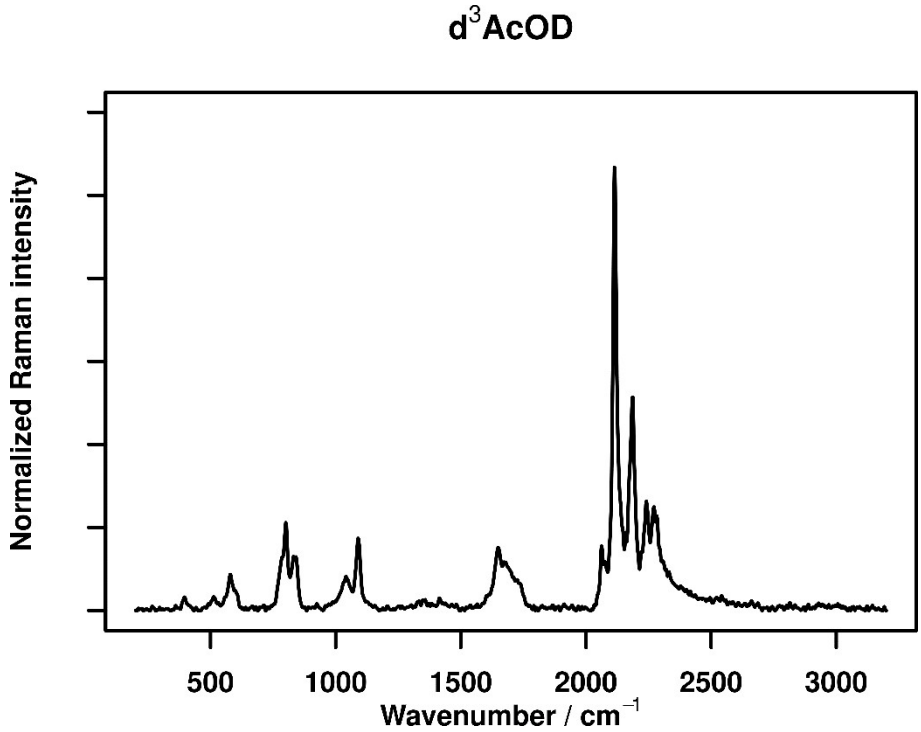

Figure S4: FT-Raman spectrum of d^3-AcOD in the range of 200 – 3200 cm^{-1}.

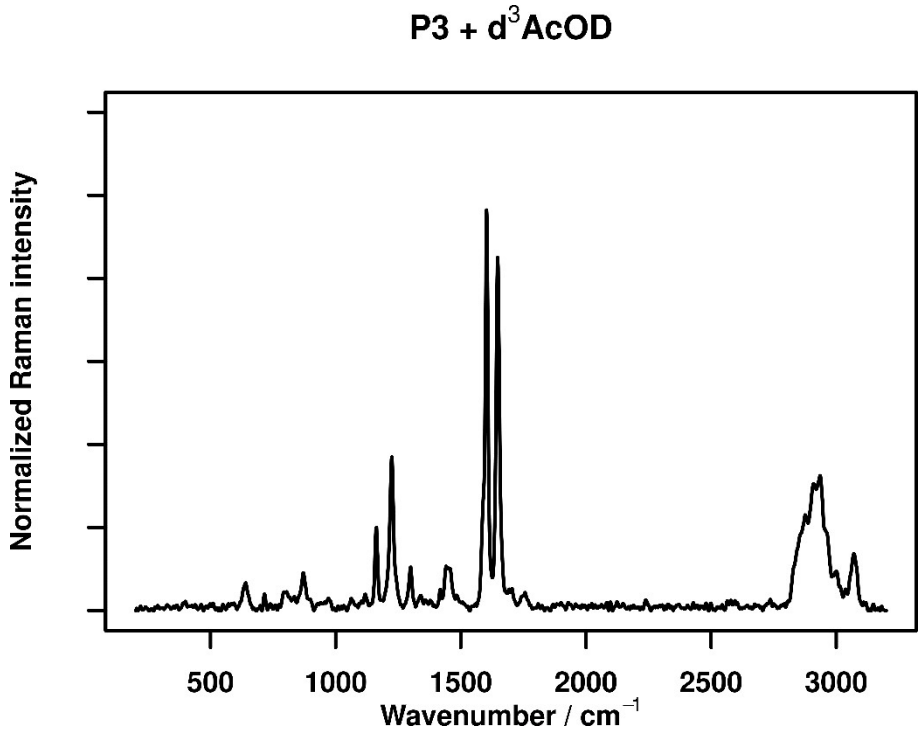

Figure S5: FT-Raman spectrum of **P3** + d^3-AcOD in the range of 200 – 3200 cm^{-1}.

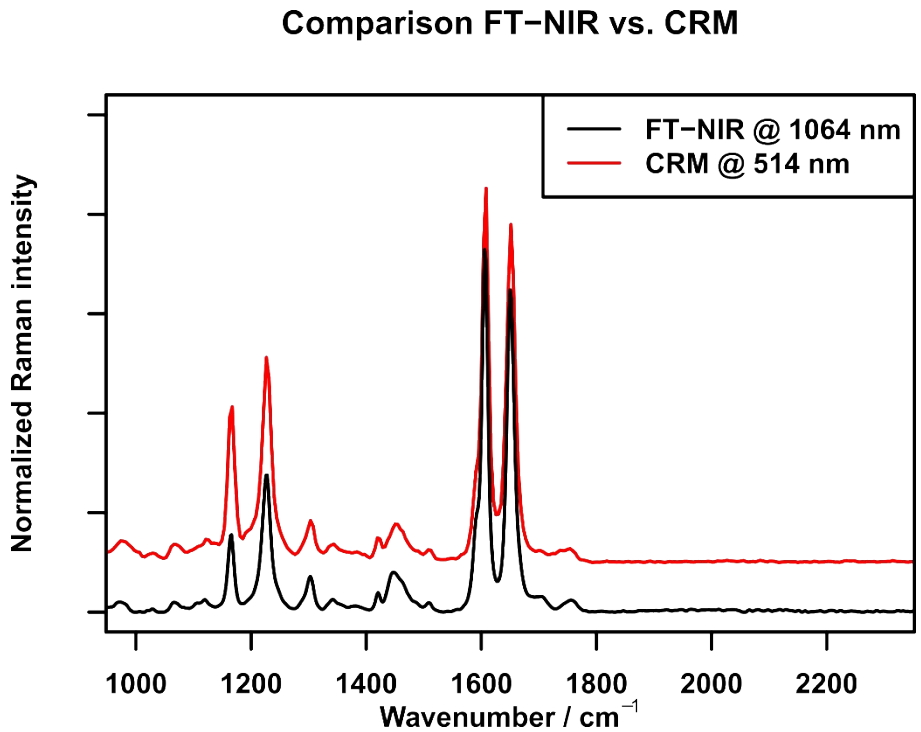

Figure S6: Comparison of the Raman spectra recorded using the FT-NIR Raman spectrometer (reference instrument) and a high quality spectrum recorded using the confocal Raman microscope (CRM)used for the spatio-temporally resolved measurements. The reference spectrum can be reproduced using the CRM, showing that no significant artifacts, e.g., fluorescence, are influencing the results.

Two-dimensional Correlation Analysis (2DCOS)

Calculation of 2DCOS maps

2DCOS was performed using in-house developed scripts in GNU R. It was performed using the principal component based approach to 2D Correlation Analysis that speeds up the calculation for larger datasets such as the spatially resolved data in this work significantly. The details of the approach have been described in previous work.[5] 2DCOS was performed over the whole timeframe of 0 to 400 s (21 measurements per point) separately on the mean spectra of each z-layer.

Additional 2DCOS maps

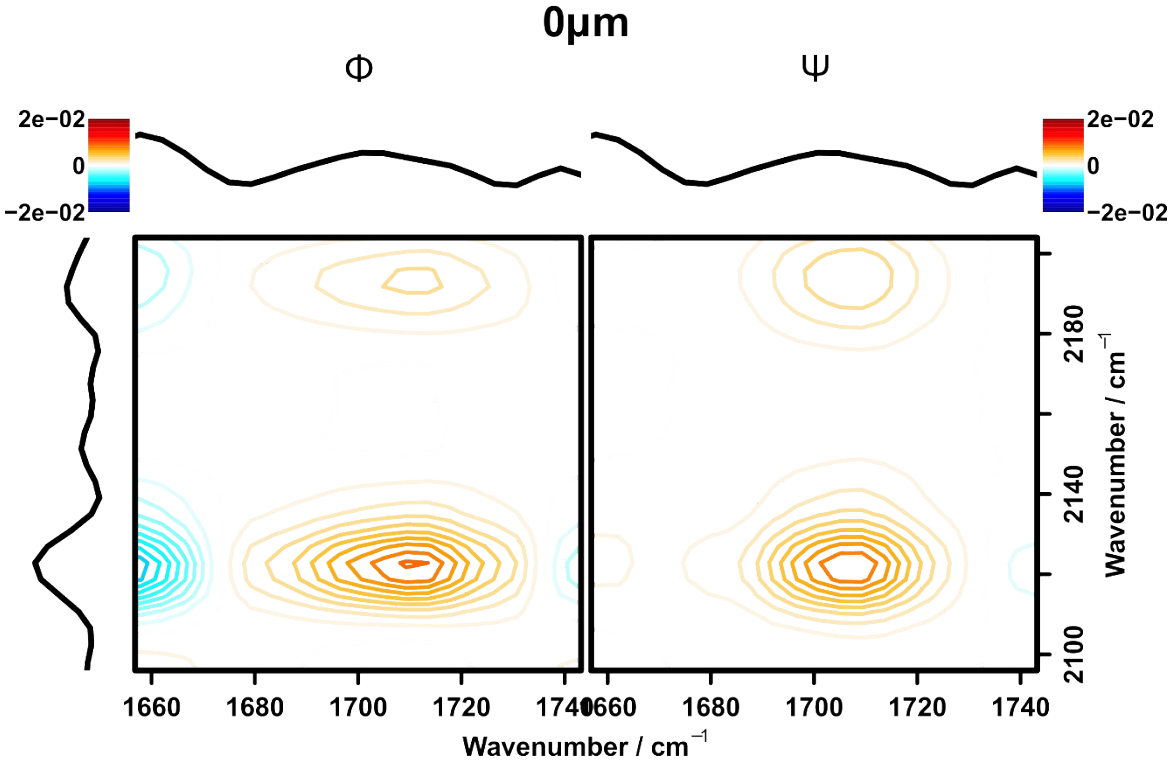

Figure S7: 2DCOS map in the area of the C-D and C=O vibration for a depth of 0 µm.

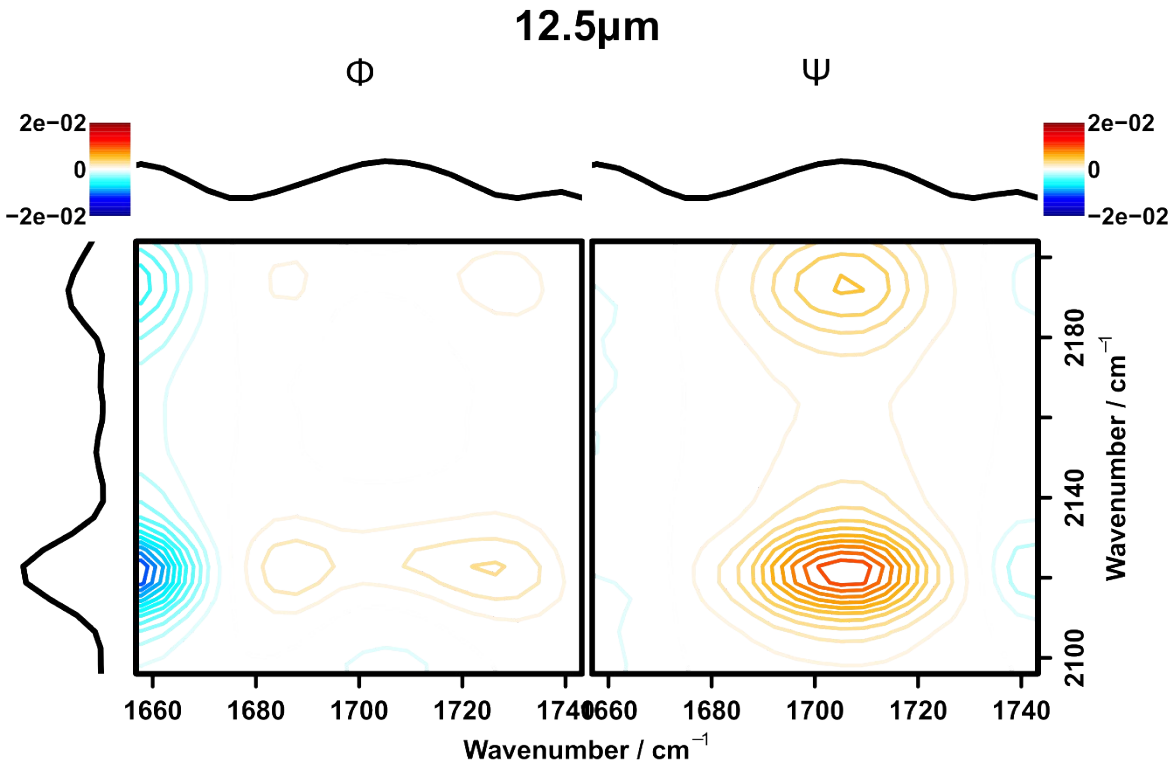

Figure S8: 2DCOS map in the area of the C-D and C=O vibration for a depth of 12.5 µm.

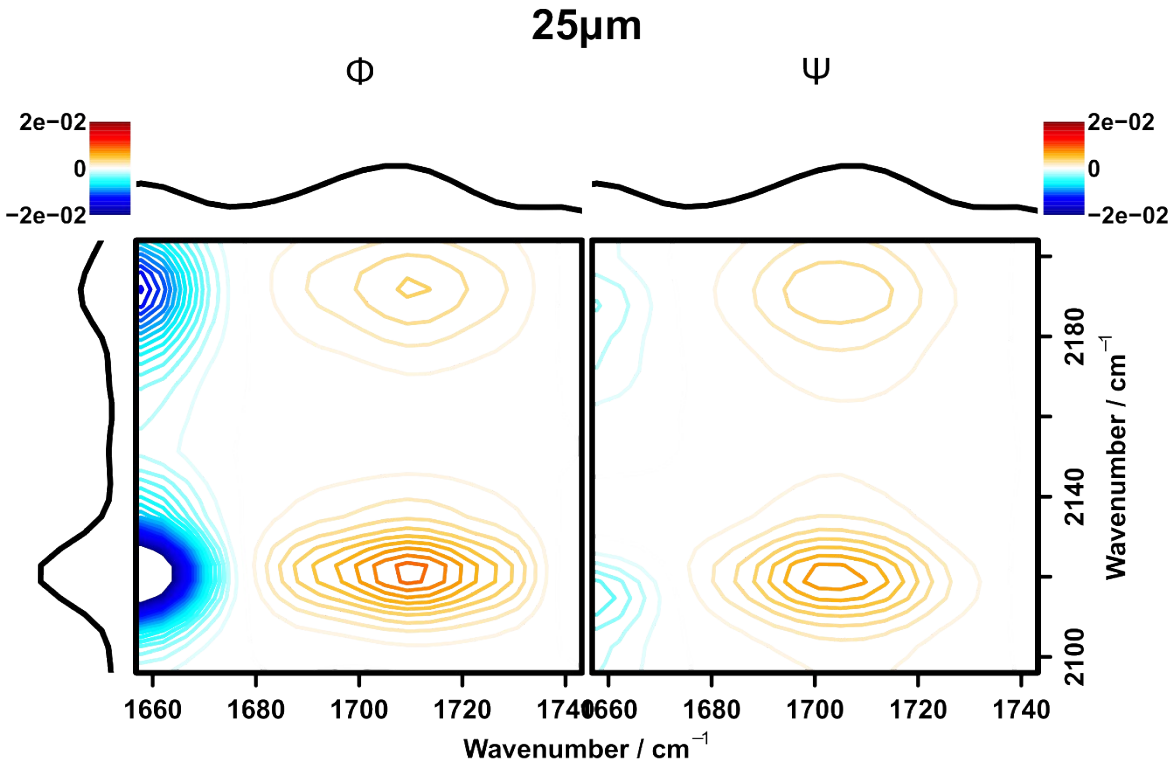

Figure S9: 2DCOS map in the area of the C-D and C=O vibration for a depth of 25 µm.

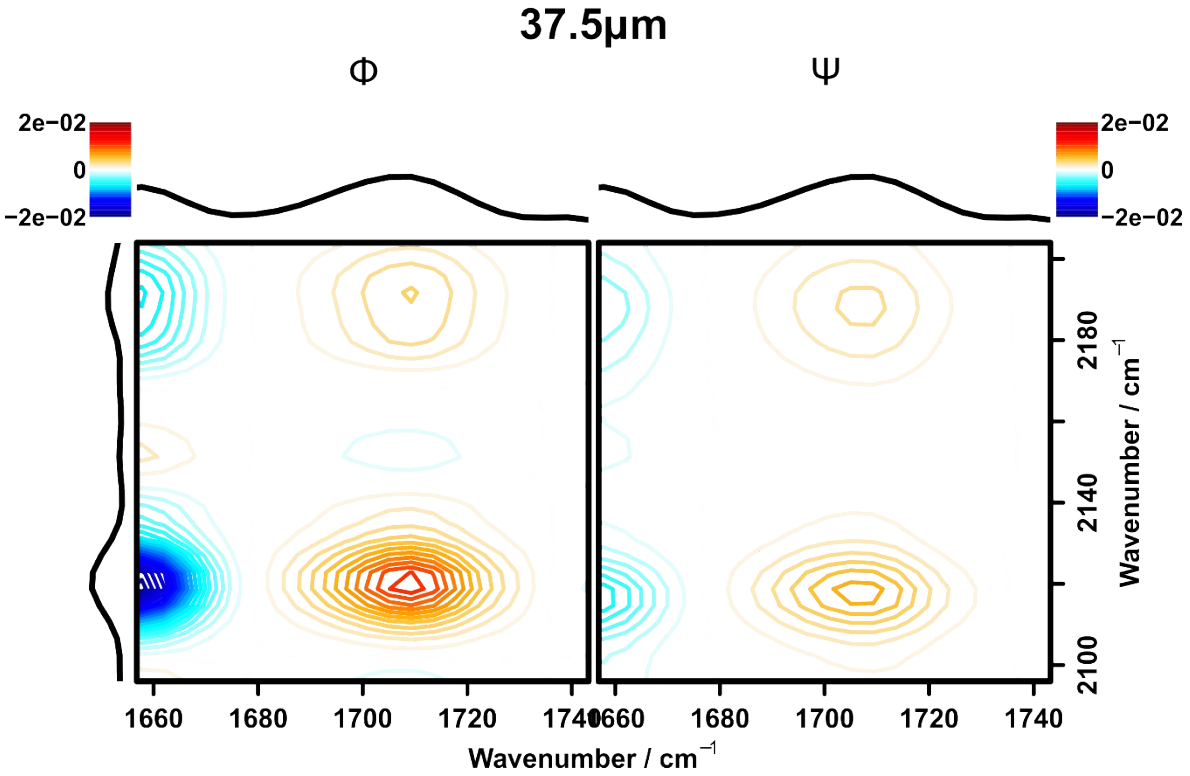

Figure S10: 2DCOS map in the area of the C-D and C=O vibration for a depth of 37.5 µm.

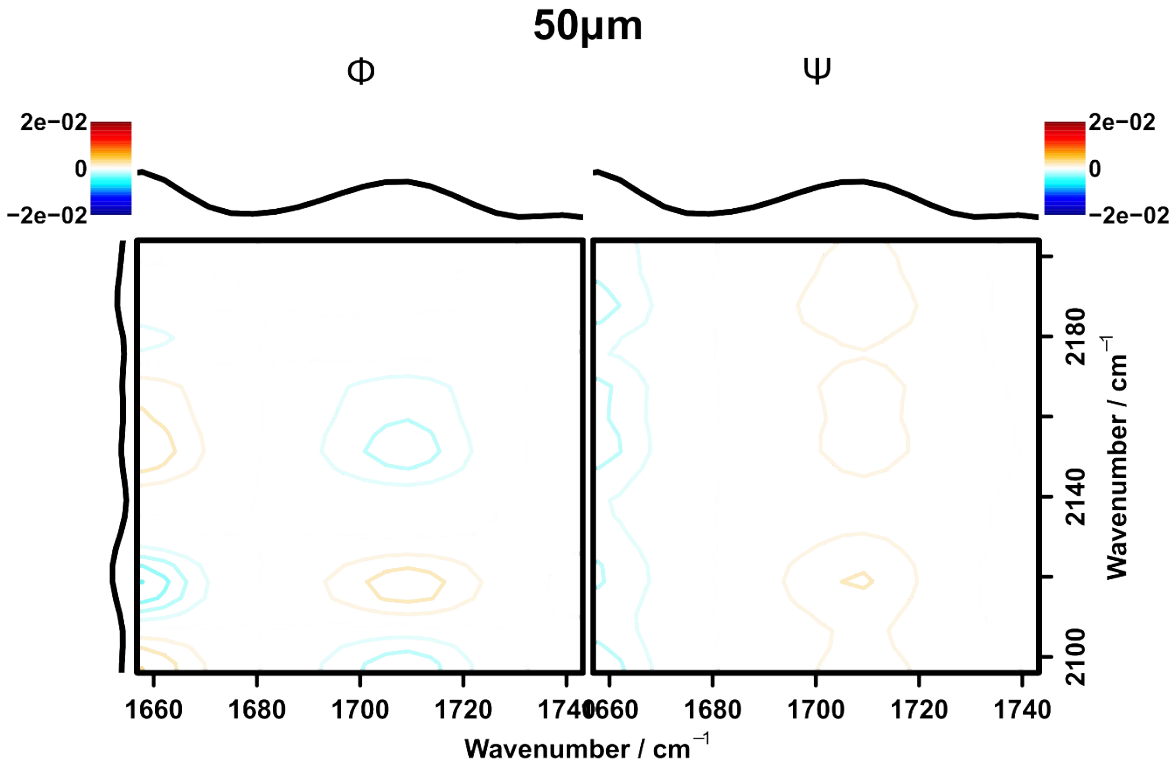

Figure S11: 2DCOS map in the area of the C-D and C=O vibration for a depth of 50 µm.

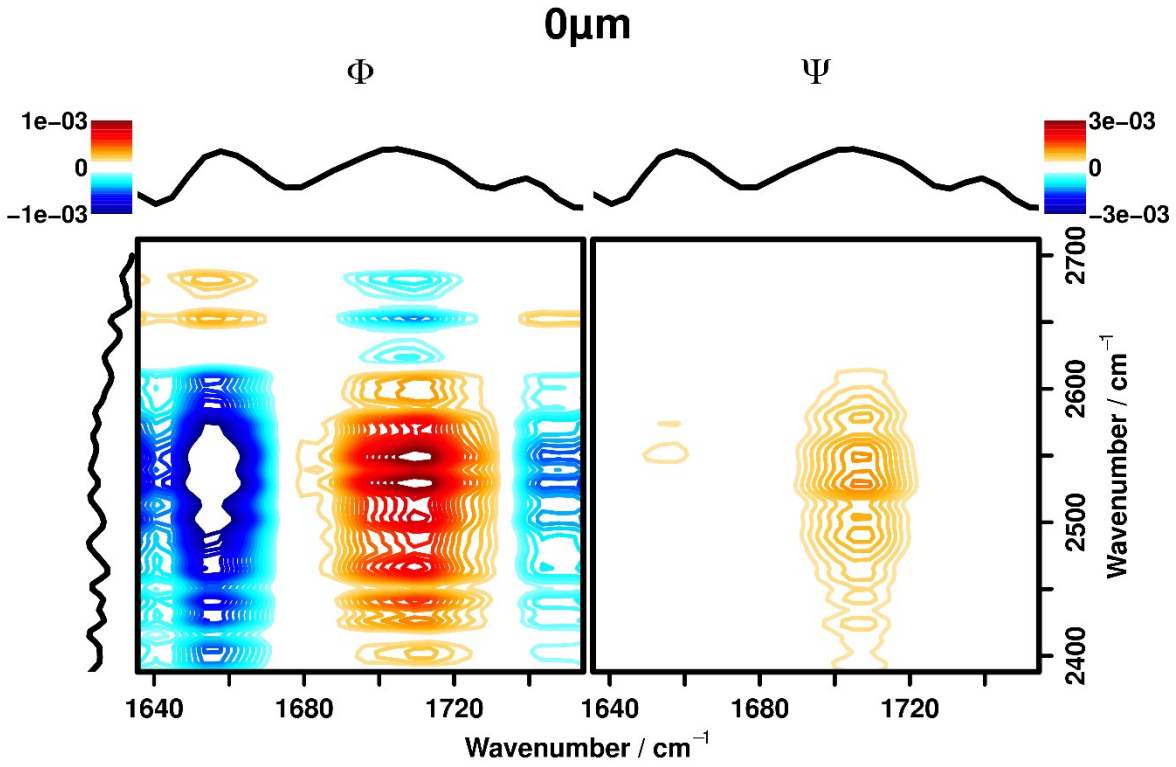

Figure S12: 2DCOS map in the area of the O-D vibration of D_2O and C=O/N vibration of the polymer for a depth of 0 µm.

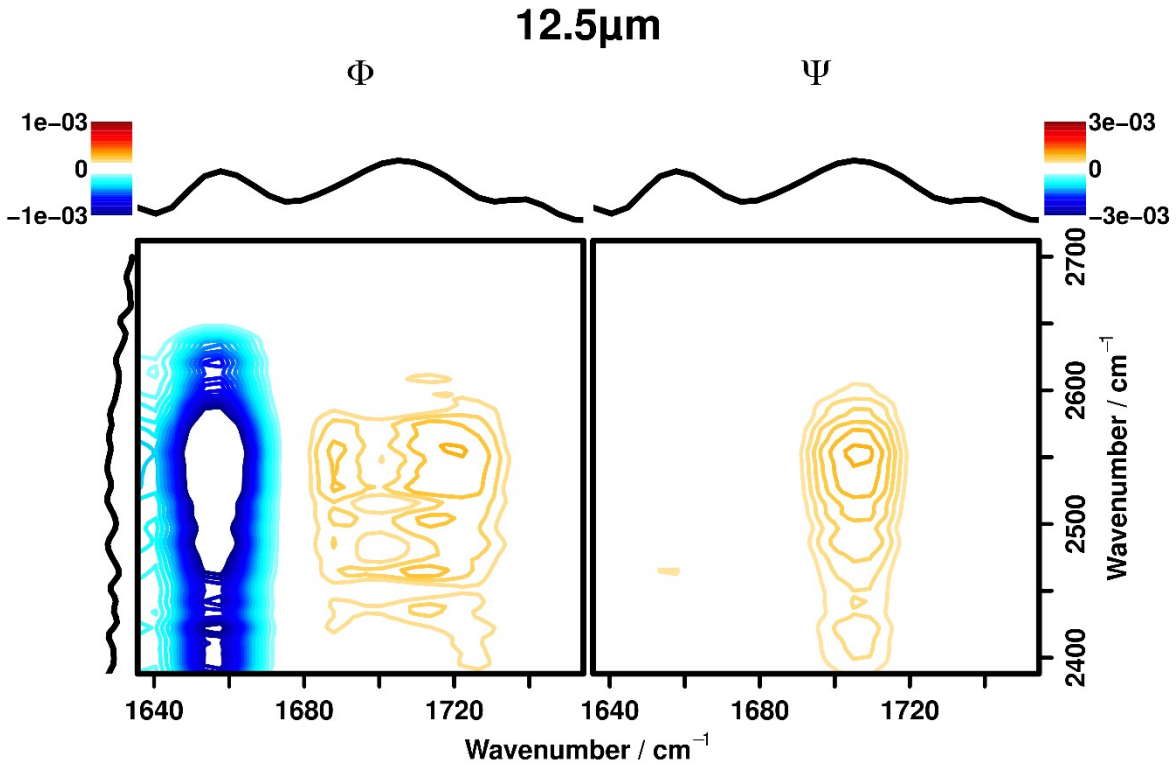

Figure S13: 2DCOS map in the area of the O-D vibration of D_2O and C=O/N vibration of the polymer for a depth of 12.5 µm.

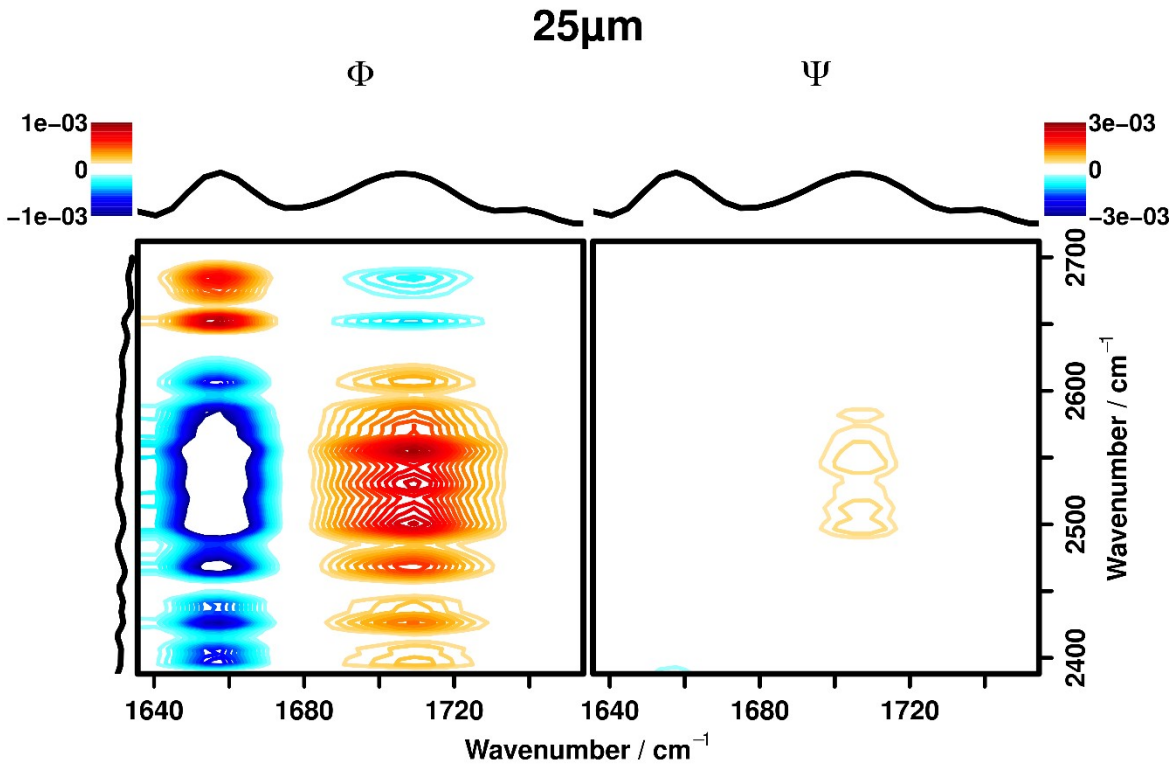

Figure S14: 2DCOS map in the area of the O-D vibration of D_2O and C=O/N vibration of the polymer for a depth of 25 µm.

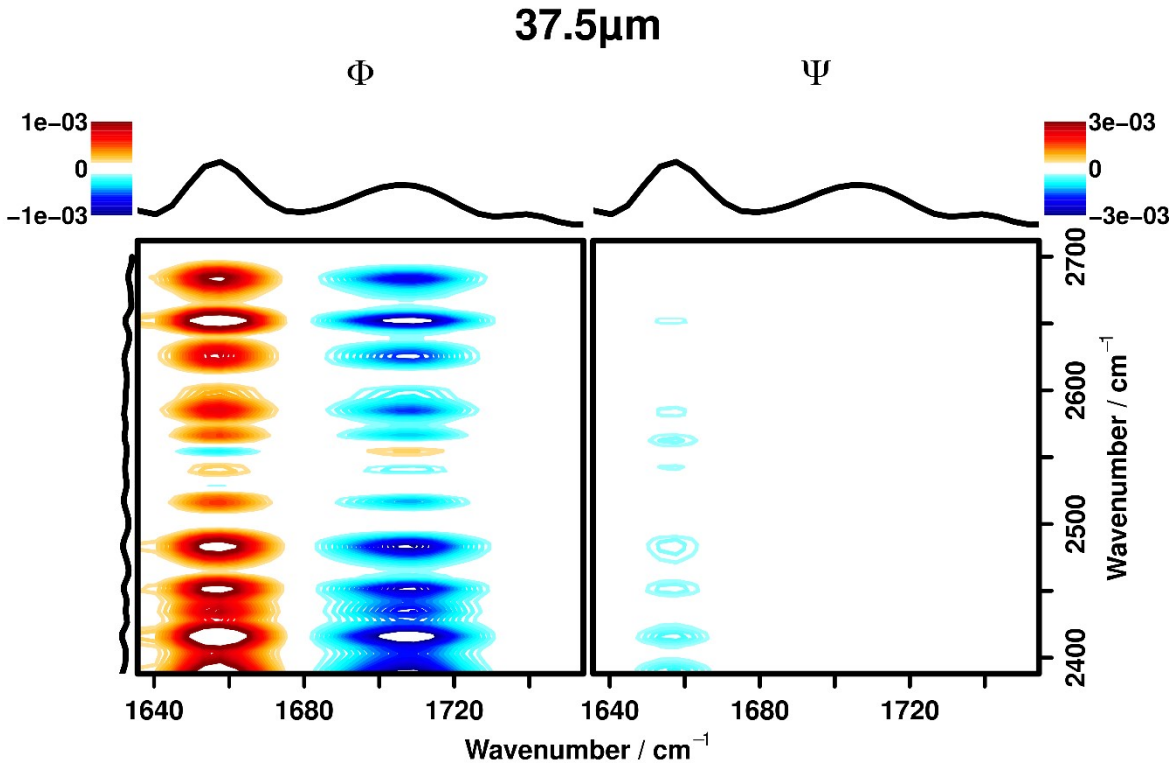

Figure S15: 2DCOS map in the area of the O-D vibration of D_2O and C=O/N vibration of the polymer for a depth of 37.5 µm.

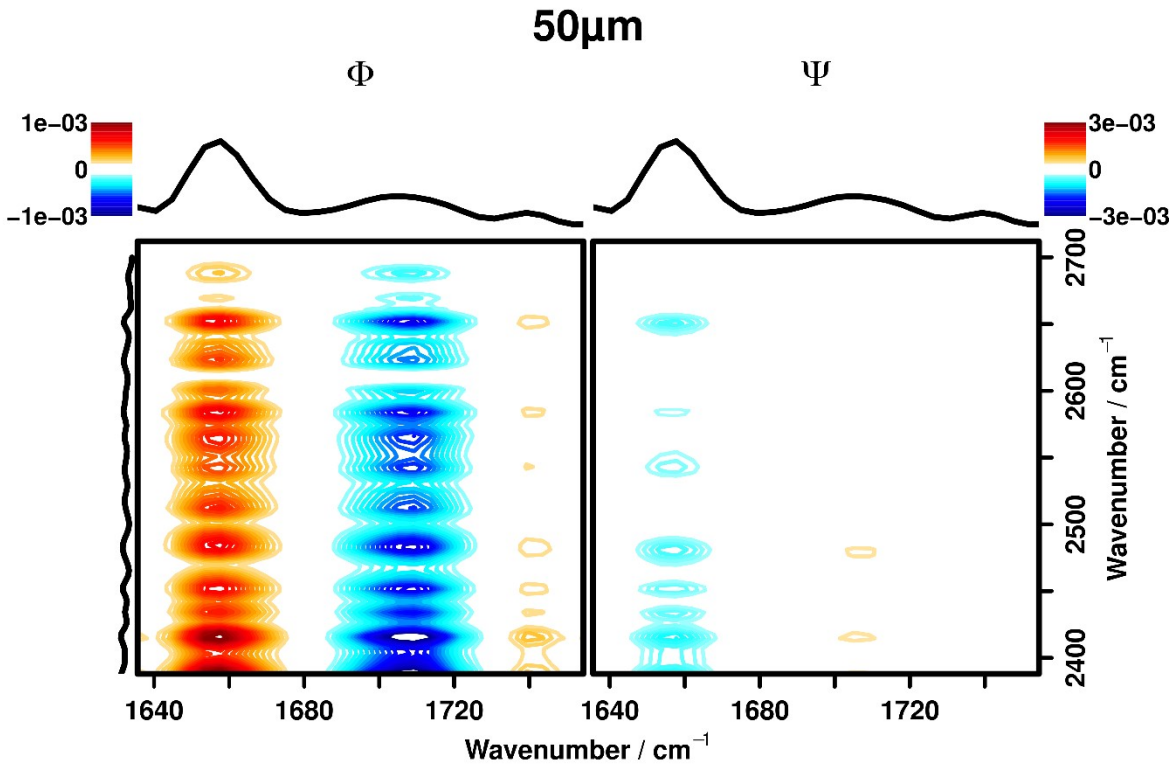

Figure S16: 2DCOS map in the area of the O-D vibration of D_2O and C=O/N vibration of the polymer for a depth of 50 µm.

Calculation of delay times

Theory and background

To calculate the time delay between the opening of the imine functionality to the aldehyde using rigorous mathematical means, an approach based on the global phase angle description of 2DCOS was used in this work. The phase angle is an important quantity in 2DCOS, that is implicitly analyzed when using Noda's rules, as it encodes the synchronicity of two signals. It is seldomly used explicitly in the analysis 2DCOS maps, although there are previous works which demonstrated the power of this approach.[6, 7]

In general, the phase angle is defined for periodic signals, such as sinus and cosine. For such signals, the phase with respect to the origin can be found by applying Fourier transform where it is encoded as the argument of the complex Fourier-domain signal:

$$f(t) = \mathrm{A} \cdot \cos\left(\omega_0 t + \phi\right) = A \cdot \cos\left(\omega_0\left(t + t_\phi\right)\right); t_\phi = \frac{\phi}{\omega_0} \tag{1}$$

$$F(\omega) = Ff(\omega) = \frac{1}{\sqrt{2\pi}}\int f(t) \cdot e^{-i\omega t} dt = \frac{A}{2} \cdot \left(e^{i\phi}\delta(\omega + \omega_0) + \epsilon \tag{2}$$

$$\begin{aligned}\arg\left(F(\omega_0)\right) &= \arctan\frac{Re\left(F(\omega_0)\right)}{Im\left(F(\omega_0)\right)} = \arctan\frac{\frac{A}{2}\cos(\phi) \cdot \left(\delta(\omega + \omega_0) + \delta(\alpha\right)}{\frac{A}{2}\sin(\phi) \cdot \left(\left(\delta(\omega - \omega_0) - \delta(\alpha\right)\right.} \\ &= \arctan(\tan\phi) = \phi\end{aligned} \tag{3}$$

As it can be seen in (3), the argument of the Fourier transformed signal at the fundamental frequency of the cosine wave is equal to the phase of the signal. This property can also be exploited to find the phase difference between two signals which can directly be related to a delay in time domain if both signals are oscillating on the same fundamental frequency (5).

$$g(t) = \mathrm{A} \cdot \cos\left(\omega_0 t + \theta\right) = A \cdot \cos\left(\omega_0\left(t + t_\theta\right)\right); t_\theta = \frac{\theta}{\omega_0} \tag{4}$$

$$\Delta T = \frac{(\theta - \delta)}{\omega_0} = \frac{\left(\arg G(\omega_0) - \arg F(\omega_0)\right)}{\omega_0} \tag{5}$$

One can derive that this phase difference is also encoded in the 2DCOS spectrum (6) of two sinusoids, which has been derived and demonstrated before.[6, 8, 9] For 2DCOS the phase difference of two signals observed at frequencies $\nu_1$and ν_2 can be obtained by getting the argument of the respective 2DCOS value (8).

$$X(\nu_1,\nu_2) = \Phi(\nu_1,\nu_2) + i \cdot \Psi(\nu_1,\nu_2) = \frac{1}{\pi T} \cdot \int_0^\infty \tilde{Y}_1(\omega) \cdot \tilde{Y}_2{}^*(\omega) d\omega \tag{6}$$

$$\tilde{Y}_i(\omega) = F\left(\tilde{y}(\nu_i,t)\right); \tilde{y}(\nu_i,t) = y(\nu_i,t) - \bar{y}(\nu_i,t) \tag{7}$$

$$for\ y(\nu_1) = f(t), y(\nu_2) = g(t): \theta - \phi = \arg\frac{\Psi(\nu_1,\nu_2)}{\Phi(\nu_1,\nu_2)} \tag{8}$$

If the signals are simple sinusoids with a fixed oscillation frequency this can again directly be related to a time-delay using (5).

Generalized 2DCOS as introduced by Noda in the 1990s exploits the Fourier Theorem that states that any (periodic) signal can be expressed as the sum of sinusoids. This theorem allows for the application of the 2DCOS formalism to arbitrary perturbations, which broadens the scope of the technique significantly. 2DCOS then correlates all Fourier components of the signals at various frequencies, which would afford a set of t = number of observations correlation spectra. This would not be feasible to analyze, so a combined value needs to be found for easy analysis of the correlation spectra. As it has been discussed before, for typical perturbation waveforms encountered in spectroscopy, the Fourier components look very similar,[9] which makes it possible to integrate over the correlation spectra of the Fourier components, which affords an average value for each pair of spectral variables. In this formalism, the phase angle encoded in the 2DCOS is not a single phase angle between two signals, but a combination of the phase angles of all Fourier components called the global phase angle.

Using the established observation, that the Fourier components of real signals are very similar, we can use this global phase angle to calculate the delay times of the Fourier components of each signal (9). Since in real life, we are dealing with discrete signals, instead of continuous Fourier transform, discrete Fourier transform, usually in form of fast Fourier transform is used. Therefore, we can think of the global phase angle of the phase angle of a cosine with the average frequency spanned by the DFT space. The frequencies in the DFT space can be calculated according to (10).

$$\Delta T(\nu_1,\nu_2) = \bar{\omega} \cdot \Delta\theta(\nu_1,\nu_2) = \bar{\omega} \cdot \arg\frac{\Psi(\nu_1,\nu_2)}{\Phi(\nu_1,\nu_2)} \tag{9}$$

$$\bar{\omega} = \frac{\sum \omega_i}{N}, \omega_i = \left[0, \frac{1}{T}, \frac{2}{T} \ldots \frac{N}{T}\right]; T = t_\infty - t_0; N = number\ of\ samples \tag{10}$$

For non-periodic signals, another problem arises here. The phase angle is fixed in the range [0, 2π] as translating a sinusoidal function by $(t + 2\pi)/\omega$ is the same as translating it by t/ω. Therefore, all angles $\Delta\theta + n \cdot 2\pi$ are valid solutions of the right-hand side of (9). For sinusoidal functions, this does not change the outcome, but for non-periodic signals, delaying a signal by t may not be the same as delaying it by $(t + 2\pi)/\omega$. Fortunately, the correct value of n can usually be found by visual inspection of the signal and, e.g., looking at the offset between the maximum values of two signals.

$$\Delta T(\nu_1,\nu_2) = \bar{\omega} \cdot (\Delta\theta(\nu_1,\nu_2) + n \cdot 2\pi) \tag{11}$$

Calculations in this work

For the application in this work the time delay between the cleavage of the imine to an aldehyde and the appearance of d³-AcOD related bands was the target for the introduced method. For this, the 2DCOS maps calculated as described above were restricted to the wavenumber region of x = 1700 - 1710 cm^{-1} (C=O band) and y = 2100 -- 2120 cm^{-1} (C-D band). Then, the global phase angles according to (9) were calculated for each point in this region (24 points in total). From these angles, the mean and standard deviations were calculated to afford the mean phase angle between the C=O and C-D signal as well as its uncertainty. Using (10) with t = 400 s (duration of the measurement) and N = 21 (number of samples), affording an $\bar{\omega}$ of 0.0275 Hz. Using $n = 0$, delay times of 4-8 seconds were obtained, which could be discarded by visual inspection. With $n = 1$, delay times between 42 and 46 seconds were obtained, which when overlaying the signals shifted by this time, visually match well to the evolution of the integrated band areas of the respective bands over time (cf. Figure S8).

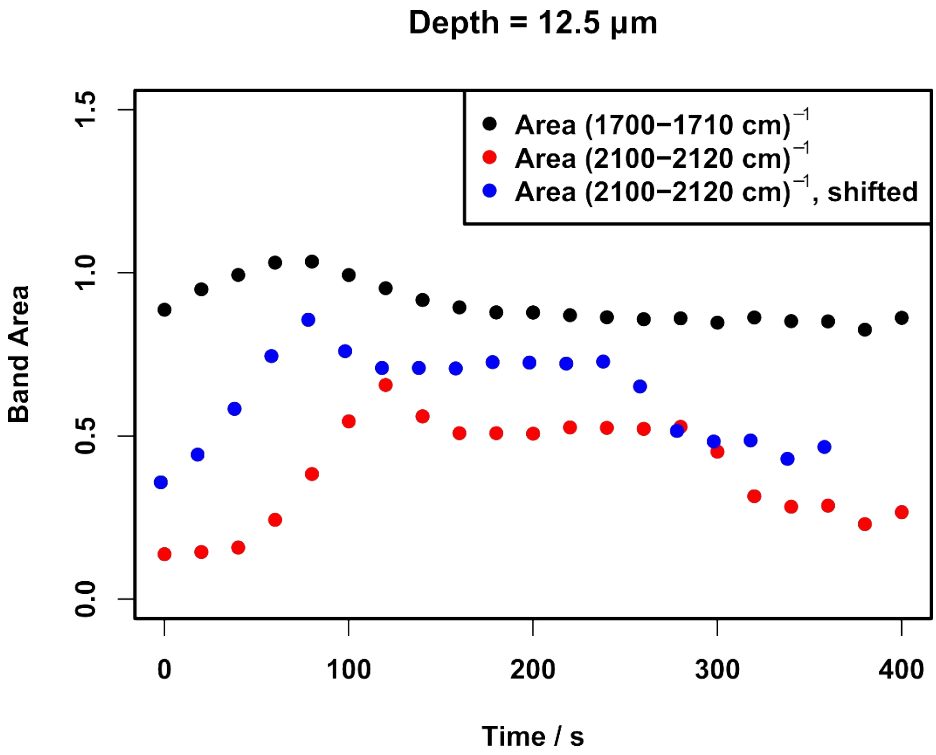

Figure S17: Visual presentation of the band areas of C=O (black, top) and C-D (bottom, red) bands as recorded originally and C-D shifted by the offset calculated *via* global phase angle (middle, blue).

Contact Angle Data

Time [s]	mean angle [°]	left angle [°]	right angle [°]	Time [s]	mean angle [°]	left angle [°]	right angle [°]
0	74.86	74.40	75.33	250	68.11	67.57	68.65
5	74.54	74.04	75.04	255	68.00	67.45	68.54
10	74.40	73.91	74.90	260	67.84	67.31	68.37
15	74.30	73.80	74.79	265	67.66	67.12	68.21
20	74.18	73.68	74.67	270	67.55	67.00	68.10
25	74.05	73.55	74.55	275	67.42	66.87	67.97
30	73.93	73.43	74.43	280	67.26	66.71	67.81
35	73.82	73.32	74.32	285	67.12	66.56	67.68
40	73.70	73.20	74.20	290	66.98	66.43	67.53
45	73.59	73.09	74.09	295	66.84	66.28	67.39
50	73.48	72.97	73.98	300	66.67	66.13	67.21
55	73.35	72.85	73.85	305	66.53	65.98	67.08
60	73.22	72.71	73.72	310	66.38	65.82	66.94
65	73.11	72.60	73.61	315	66.23	65.68	66.77
70	72.97	72.46	73.49	320	66.09	65.54	66.64
75	72.84	72.33	73.35	325	65.92	65.36	66.48
80	72.72	72.20	73.23	330	65.75	65.19	66.31
85	72.59	72.07	73.11	335	65.61	65.04	66.18
90	72.47	71.95	72.99	340	65.48	64.91	66.04
95	72.34	71.82	72.86	345	65.32	64.77	65.88
100	72.22	71.70	72.73	350	65.19	64.63	65.75
105	72.09	71.57	72.61	355	65.05	64.49	65.61
110	71.96	71.45	72.47	360	64.90	64.35	65.45
115	71.83	71.31	72.34	365	64.75	64.20	65.29
120	71.71	71.19	72.23	370	64.60	64.03	65.16
Time	**mean angle**	**left angle**	**right angle**	**Time**	**mean angle**	**left angle**	**right angle**

[s]	[°]	[°]	[°]	[s]	[°]	[°]	[°]
125	71.59	71.08	72.10	375	64.44	63.88	64.99
130	71.44	70.91	71.96	380	64.29	63.73	64.85
135	71.32	70.79	71.84	385	64.13	63.58	64.68
140	71.19	70.67	71.71	390	63.95	63.40	64.50
145	71.05	70.53	71.57	395	63.82	63.26	64.39
150	70.92	70.40	71.45	400	63.65	63.09	64.21
155	70.77	70.25	71.30	405	63.50	62.95	64.05
160	70.66	70.13	71.18	410	63.32	62.76	63.89
165	70.54	70.02	71.07	415	63.19	62.63	63.75
170	70.39	69.87	70.91	420	63.03	62.46	63.59
175	70.27	69.73	70.81	425	62.82	62.26	63.39
180	70.13	69.60	70.66	430	62.67	62.11	63.22
185	69.98	69.45	70.52	435	62.52	61.95	63.08
190	69.86	69.32	70.39	440	62.37	61.82	62.93
195	69.69	69.16	70.22	445	62.20	61.63	62.77
200	69.54	68.99	70.09	450	62.04	61.48	62.60
205	69.41	68.87	69.95	455	61.88	61.31	62.44
210	69.23	68.68	69.77	460	61.72	61.16	62.28
215	69.12	68.58	69.67	465	61.55	60.98	62.11
220	68.97	68.44	69.51	470	61.41	60.85	61.98
225	68.83	68.27	69.38	475	61.27	60.71	61.83
230	68.70	68.17	69.24	480	61.09	60.53	61.64
235	68.54	67.99	69.08	485	60.91	60.35	61.47
240	68.42	67.87	68.98	490	60.77	60.20	61.33
245	68.28	67.73	68.84				

References

1. N. Kuhl, S. Bode, R. K. Bose, J. Vitz, A. Seifert, S. Hoeppener, S. J. Garcia, S. Spange, S. van der Zwaag, M. D. Hager and U. S. Schubert, Acylhydrazones as Reversible Covalent Crosslinkers for Self-Healing Polymers, *Adv. Funct. Mater.*, 2015, **25**, 3295-3301.
2. B. García-Acosta, F. García, J. M. García, R. Martínez-Máñez, F. Sancenón, N. San-José and J. Soto, Chromogenic Signaling of Hydrogen Carbonate Anion with Pyrylium-Containing Polymers, *Org. Lett.*, 2007, **9**, 2429-2432.
3. R Core Team, *R: A Language and Environment for Statistical Computing*, R Foundation for Statistical Computing, 2022.
4. C. G. Ryan, E. Clayton, W. L. Griffin, S. H. Sie and D. R. Cousens, SNIP, a statistics-sensitive background treatment for the quantitative analysis of PIXE spectra in geoscience applications, *Nuclear Instruments and Methods in Physics Research Section B: Beam Interactions with Materials and Atoms*, 1988, **34**, 396-402.
5. J. Hniopek, M. Schmitt, J. Popp and T. Bocklitz, PC 2D-COS: A Principal Component Base Approach to Two-Dimensional Correlation Spectroscopy, *Appl. Spectrosc.*, 2020, **74**, 460-472.
6. S.-I. Morita, Y. Ozaki and I. Noda, Global Phase Angle Description of Generalized Two-Dimensional Correlation Spectroscopy: 1. Theory and its Simulation for Practical Use, *Appl. Spectrosc.*, 2001, **55**, 1618-1621.
7. S.-I. Morita, Y. Ozaki and I. Noda, Global Phase Angle Description of Generalized Two-Dimensional Correlation Spectroscopy: 2. Its Application to Temperature-Dependent Infrared Spectra of a Langmuir—Blodgett Film of 2-Dodecyl-7,7,8,8-Tetracyanoquinodimethane, *Appl. Spectrosc.*, 2001, **55**, 1622-1627.
8. I. Noda, Techniques useful in two-dimensional correlation and codistribution spectroscopy (2DCOS and 2DCDS) analyses, *J. Mol. Struct.*, 2016, **1124**, 29-41.
9. I. Noda, Close-up view on the inner workings of two-dimensional correlation spectroscopy, *Vib. Spectrosc*, 2012, **60**, 146-153.